THE ROYAL SOCIETY
PUBLISHING

Finite-element model of the active organ of Corti

Guangjian Ni[1], Stephen J. Elliott[1] and Johannes Baumgart[2]

[1]Institute of Sound and Vibration Research, University of Southampton, Highfield Campus, Southampton SO17 1BJ, UK
[2]Max Planck Institute for the Physics of Complex Systems, Nöthnitzer Strasse 38, 01187 Dresden, Germany

GN, 0000-0002-9240-3020

The cochlear amplifier that provides our hearing with its extraordinary sensitivity and selectivity is thought to be the result of an active biomechanical process within the sensory auditory organ, the organ of Corti. Although imaging techniques are developing rapidly, it is not currently possible, in a fully active cochlea, to obtain detailed measurements of the motion of individual elements within a cross section of the organ of Corti. This motion is predicted using a two-dimensional finite-element model. The various solid components are modelled using elastic elements, the outer hair cells (OHCs) as piezoelectric elements and the perilymph and endolymph as viscous and nearly incompressible fluid elements. The model is validated by comparison with existing measurements of the motions within the passive organ of Corti, calculated when it is driven either acoustically, by the fluid pressure or electrically, by excitation of the OHCs. The transverse basilar membrane (BM) motion and the shearing motion between the tectorial membrane and the reticular lamina are calculated for these two excitation modes. The fully active response of the BM to acoustic excitation is predicted using a linear superposition of the calculated responses and an assumed frequency response for the OHC feedback.

1. Introduction

The overall dynamics of the cochlea are characterized by the travelling wave theory [1,2], in which a slow wave, due to the interaction between the stiffness of the basilar membrane (BM) and the inertia of the fluid in the chambers, propagates along the cochlea, from the basal to the apical end when the stapes is driven by an external pressure. The amplitude of the travelling wave gradually increases, and the wave speed gradually decreases as the BM stiffness reduces along the length of the cochlea, until it reaches a frequency-dependent position, called the characteristic place, where the BM resonates at the excitation frequency, after which it decays rapidly. The amplitude of the travelling wave at the characteristic place is also enhanced, by about 40 dB or more, by the action of the cochlear amplifier within the organ of Corti, which is believed to be associated with a feedback loop driven by the electromotility of the outer hair cells (OHCs) [3].

The precise micromechanical mechanism of the amplification within the active cochlea is not fully understood as it is difficult to identify the different contributions of the various cell types [3]. Non-invasive measurements of the internal motion within the organ of Corti are difficult, particularly *in vivo* in the fully active cochlea [4], but measurements with acoustic excitation of the partly active cochlea [5–8] are possible. Experimental observations of internal motion of the organ of Corti using *in vivo* or *in vitro* preparations have been reported, for acoustic excitation, by Nilsen & Russell [5], and Lee *et al.* [9], by Nowotny & Gummer [9,10] for electrical excitation, by Chan & Hudspeth [11] for both excitation modes and by Fridberger *et al.* [6] for static pressure loading. Even though there is still some debate about the role of the hair bundle dynamics [12–18], it is widely believed that it is mainly the somatic

motility of the OHCs that provides the power to drive the amplification of the vibration within the mammalian organ of Corti [3,19].

Cochlear models are useful to connect our understanding of the mechanics of the cochlea with incomplete experimental observations. Modelling the mechanics of the cochlea allows us to test assumptions about cochlear function, by comparing responses predicted using models with experimental observations. With a properly constructed cochlear model, we are also able to carry out experiments *in silico*, from which we can predict the output response to stimuli without the imperfections due to an experimental set-up. The key question with any model, however, is the degree of detail that must be included to simulate the behaviour of interest. There are also difficulties in extrapolating directly from experimental observations made *in vitro* and *in situ* to the normal operation of the intact organ *in vivo* [20].

A pioneering micromechanical model of the cochlea with simplified cellular and membrane components of the organ of Corti embedded was developed by Kolston & Ashmore [21], using the finite-element method, in which the OHC activity was modelled by introducing a force acting at the two ends of the OHCs and the force was determined by the shear displacement between the reticular lamina (RL) and tectorial membrane (TM). Similarly, Nam & Fettiplace [22] developed an elastic micromechanical model of the organ of Corti to study force transmission and elastic wave propagation [23], in which OHC somatic and hair bundle active forces were both considered. Developments of the finite-element method and in computational power have allowed newer models to study wave propagation in the cochlear partition [23–25], mechanical effects of OHC somatic and hair bundle motility [22,26], fluid–solid interaction [27,28] and detailed motion patterns within the organ of Corti in response to static pressure loading [29]. The active amplification process within the cochlea has also been studied using either lumped-parameter models [30–32], or simplified three-dimensional models [21,33–36]. The detailed structures of the organ of Corti are not fully represented in those models, however, and some do not model the effect of the cochlear fluids [22,23]. The main contribution of the present work is to provide some initial predictions of the detailed motion pattern within the organ of Corti in the active case, based on a model that is validated using the available experimental data on passive acoustic or entirely electrical excitation.

The organ of Corti consists of a multitude of different specialized cells, which provide the setting of our highly sensitive and selective hearing. All cells are filled and surrounded by fluid. To account for this, we discretize the volume material by the finite-element method and so ensure local force, torque and mass balance. The work presented here is the first model to implement a feedback loop in a finite-element model of the cochlea that includes a detailed organ of Corti geometry as well as fluid–structure interaction, and hence to predict the internal motion within the organ of Corti for acoustic stimulation in the fully active case. The advantage of the finite-element method is its capacity to model structures having complex geometry. In this paper, a finite-element model of a slice of the guinea pig cochlea is constructed, based on the two-dimensional anatomy for the apical end in the guinea pig that was originally used by Baumgart *et al.* [37] to study

motion within the organ of Corti in response to somatic electromechanical forces from the OHCs. The micromechanical model of the organ of Corti is built at micrometre level, with the finite-element software ANSYS (v. 15.0, 2014). We use the plane element, plane183, for elastic components, a user-defined viscous fluid element [38,39] for the perilymph and endolymph, the piezoelectric element, plane223, for OHCs walls and the beam element, beam188, for the Deiters cell rods and the stereocilia. We do not use the fluid79 element, as it introduces significant elastic stiffness for shear and rotational strains. The longitudinal fluid flow in the inner sulcus will add some pressure load on the BM and on the other neighbouring cells in this area, but is excluded here due to the restrictions of a two-dimensional model. If the organ of Corti itself is assumed to be longitudinally locally reacting, however, then the model can be used to predict its mechanical admittance at a given position along the cochlea, which could be incorporated into coupled models that include the longitudinal fluid coupling [40,41].

The motion within the organ of Corti is first simulated in response to a static pressure loading on the BM, for comparison with the experimental measurements of Fridberger *et al.* [6]. Then, the BM motion and the shearing motion between the TM and RL are calculated when the slice is driven either acoustically or electrically, and these results are also compared with previous experimental observations [5,9–11]. The fully active response of the BM to acoustic excitation is then predicted, assuming small displacements, using a linear superposition of the calculated responses, with feedback provided by an appropriately defined gain function for the OHCs.

2. Finite-element model

2.1. Model description

The cochlea cross section has a rich and multi-scaled geometry. The overall cross section has dimensions of the order of millimetres, with the hair cells and supporting cells being on the micrometre scale [42] and the stereocilia being of the order of fractions of a micrometre. To handle the geometric complexity, we employ the finite-element method. A numerical two-dimensional model has been built, based on geometry from the guinea pig cochlea at a place corresponding to the characteristic frequency of about 0.8 kHz [37].

The dynamics of the cochlea is characterized by values of the Reynolds number well below one; furthermore, the organ of Corti moves by only a very small fraction of its size [4]. Therefore, the nonlinearities originating from large deformations, which are important in most classical engineering problems involving flows, can be neglected here. This allows us to ignore convective and finite-displacements effects, and thus we have to solve only the linear problem for the mechanics for small oscillations. As the frequencies are high, we retain the inertial term. An efficient approach to computing the linear and strongly coupled fluid–structure interaction problem in this complex geometry is the method employed by Kozlov *et al.* [38] to study the mechanics of the hair bundle in its viscous environment in three dimensions. Here, we use this monolithic approach for the displacement and pressure variables in two dimensions. This approach differs from Baumgart *et al.* [37] as we do not condense out the pressure degree of freedom on the element level.
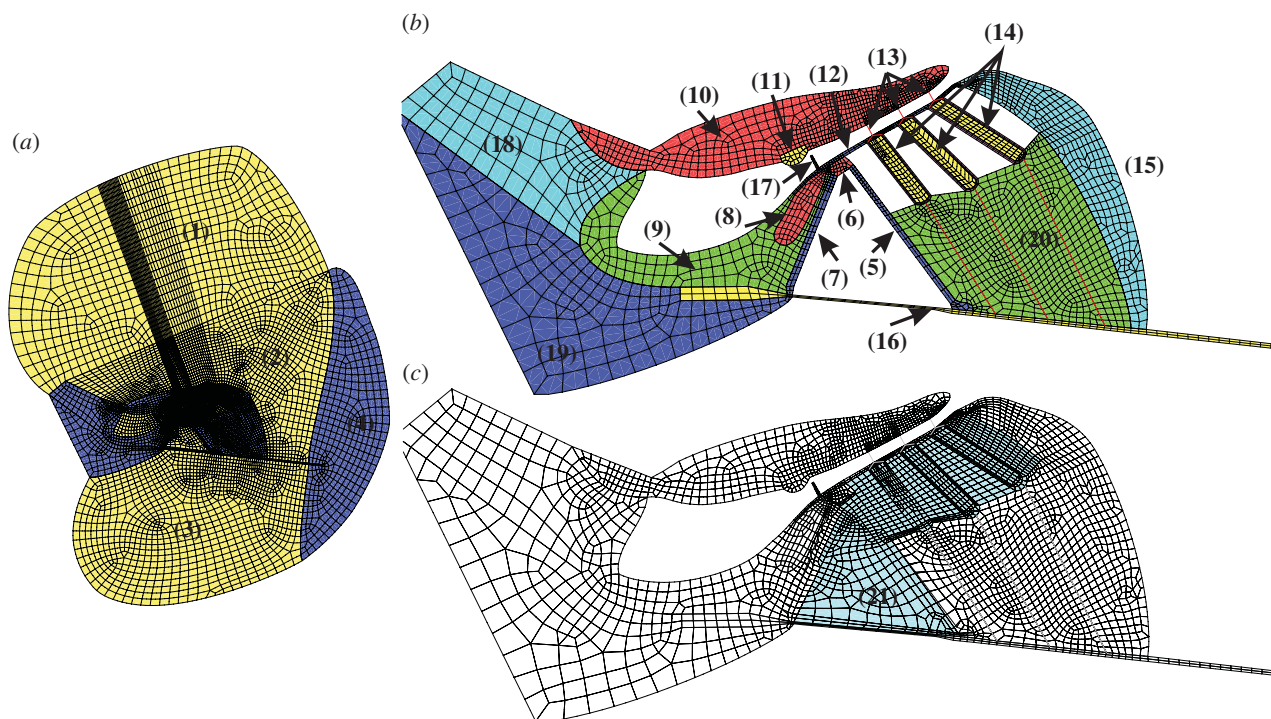
Figure 1. Finite-element model of a cochlear slice (*a*) taken from a position whose characteristic frequency is about 0.8 kHz in the guinea pig, which was constructed in Ansys (v. 15.0, 2014), together with a zoomed in view of the elastic components (*b*) and (*c*) illustration of the second domain filled with fluid. (1) Scala vestibuli, (2) scala media, (3) scala tympani, (4) spiral ligament, (5) outer pillar cell, (6) pillar cell head, (7) inner pillar cell, (8) inner hair cell, (9) inner sulcus cells, (10) tectorial membrane, (11) Hensen stripe, (12) reticular lamina, (13) outer hair cells stereocilia, (14) outer hair cells, (15) Hensen cells, (16) basilar membrane, (17) inner hair cell stereocilia, (18) spiral limbus, (19) spiral lamina, (20) Deiters cells and (21) fluid filled region. The highly rigid cytoskeleton in the Deiters cells region is modelled with beam element, which is referred to as the Deiters cell rod in this paper.

For the linear mechanics, the momentum balance of the Newtonian fluid reads

$$\rho_f \frac{\partial \mathbf{v}}{\partial t} = -\nabla p + \eta \nabla \cdot \left[(\nabla \mathbf{v} + (\nabla \mathbf{v})^{\mathrm{T}}) - \frac{2}{3} \nabla \cdot \mathbf{v} \mathbf{I} \right],$$

$$\text{with } \mathbf{v} = \frac{\partial \mathbf{u}}{\partial t},$$
(2.1)

where t is time, ρ_f is the fluid density, p is the pressure, $\mathbf{v}$ is the velocity vector, $\mathbf{u}$ is the displacement vector, η is the dynamic viscosity and $\mathbf{I}$ stands for the second-order identity tensor. This description must be complemented by a constitutive equation, which is given here by the linear relation between pressure and displacement to express the compressibility of the fluid, with the bulk modulus K, as

$$p = -K \nabla \cdot \mathbf{u}.$$
(2.2)

For the elastic elements, we solve the equation for an isotropic elastic material

$$\rho_s \frac{\partial^2 \mathbf{u}}{\partial t^2} = \nabla \cdot \left[\frac{E}{(1+v)} (\nabla \mathbf{u} + (\nabla \mathbf{u})^{\mathrm{T}}) + \frac{Ev}{(1+v)(1-2v)} \nabla \cdot \mathbf{u} \mathbf{I} \right], \quad (2.3)$$

with the solid density ρ_s, the Young's modulus E and the Poisson's ratio v as material properties. Damping of the elastic material is implemented by a damping matrix, which is proportional to the stiffness matrix.

The finite-element method is employed to solve the equations above for the fluid and solid materials within the cochlear cross section. For the fluid, the pressure is approximated by linear basis functions and the displacement by quadratic basis functions. The basis functions have nodes at the corners and for the displacements also at the mid-

points of the edges of the element. The implementation follows Zienkiewicz *et al.* [43] for the two-field incompressible elasticity. As the mechanical problem we have to solve is linear, we use a harmonic time dependence of the form $e^{i\omega t}$ for the time derivatives involved, where i is the imaginary unit and ω is the angular frequency. This allows us to formulate the problem in the frequency domain. Using a weak formulation and a discretization with the shape functions, the system of equations for the fluid and solid domain can be written in one matrix equation as

$$(-\omega^2 \mathbf{M} + i\omega \mathbf{C} + \mathbf{K})\mathbf{w} = \mathbf{f},$$
(2.4)

where $\mathbf{M}$, $\mathbf{C}$ and $\mathbf{K}$ are the mass, damping and stiffness matrices, respectively. The vector $\mathbf{w}$ contains the displacement degrees of freedom for the whole domain, the pressure field in the fluid domain and the voltage, and the vector $\mathbf{f}$ represents the external excitation forces. The coupling of all degrees of freedom represents a monolithic approach to solve the fluid–structure interaction problem.

There can be fluid flow in the radial direction through the OHCs and outer pillar cells. To take this into account, we model the region surrounded by the RL, inner sulcus, BM, Deiters cells and Hensen cells by two domains, representing the structure and the fluid respectively, which are coupled to give the overall finite-element model. Similarly, the fluid flow in the subtectorial space is not impeded by the presence of the OHC stereocilia, because these are modelled as beams, and these degrees of freedom are not coupled to the fluid. The first domain includes the pillar cells and OHCs and the second one the fluid filling of the shaded region, as shown in figure 1*c*. The two-dimensional model of the cochlea

consists of 3095 elements for the elastic components, 5525 elements for the fluid, 18 beam elements for the Deiters cell rods and the stereocilia on top of the OHCs, 216 piezoelectric elements for the OHCs walls, and has in total 26 631 nodes. The discretized geometry is depicted in figure 1.

At the position where the geometry is obtained, the BM is connected to the spiral lamina on its left-hand side and with the spiral ligament on the other side. The *in vivo* boundary conditions for the BM are complicated and depend on neighbouring tissues and fibres. Homer *et al.* [44] show that a simple beam model of the BM is capable of simulating the BM deflection profile observed by Cooper [45] at all frequencies. For their model, the BM is simply supported at the left end (at the spiral lamina) and clamped at the other end (at the spiral ligament). Steele & Puria [46] clamped both ends in their two-dimensional finite-element model of the organ of Corti and emphasized that the clamping on the right side of the BM is important for the guinea pig. Ni & Elliott [47] showed that the fluid coupling and the coupled response are not critically dependent on the BM boundary conditions and the fluid coupling in cochlear models can be reasonably well estimated by assuming a single, fixed, radial profile. We assume here that the BM of the present model is clamped at its two ends, which is consistent with the model of Steele & Puria [46]. For the fluid elements used here, the outer edges in the scala vestibuli and scala tympani are implicitly pressure release, to reflect the openings generally required when the experimental measurements, used to validate the model, were made in excised cochlear sections.

2.2. Material properties

The elastic moduli of the different cell types vary by several orders of magnitude. For example, the modulus of TM is of the order of kilopascals in the apical turn [27], but the bone of the partition and walls is of the order of gigapascals [48]. Generally, with knowledge of the protein fibres and their arrangement, an estimate can be made for the effective stretching and bending stiffness of a particular component. However, uncertainty remains, for example, in the volume fraction of protein in a particular component, the cross-links and in the stiffness of the ground substance. The important material properties of the model used here are listed in table 1, which are tuned to obtain the resonant frequency which is the same as the corresponding characteristic frequency, and are within the range of measurements and models reported by Cai & Chadwick [27], Steele & Puria [46], Scherer & Gummer [49], Strelioff & Flock [50] and Frank *et al.* [51]. The parameters were manually adjusted and an order of magnitude estimate was usually sufficient, as the response of the model was robust to smaller variation in these parameters.

Poisson's ratio of components is taken to be $v = 1/2 - E/6K$, where E is Young's modulus of each elastic component and the bulk modulus of the fluid, K, is equal to 1 GPa. The density for all components is similar to water; $1 \times 10^3 \ \mathrm{kg \ m^{-3}}$. The factor used to obtain the damping from the stiffness matrix is 0.1 for all elastic components. This was tuned to the typical phase change over frequency of a travelling wave near the resonant frequency. The dynamic viscosity of the cochlear fluid is set to 1 mPa·s and its bulk modulus is equal to 1 GPa. The OHCs are modelled with a piezoelectric wall and are filled with fluid. In practice, the material properties will depend on many factors and would

Table 1. Material properties of some elastic elements in the finite-element slice model.

components	Young's modulus [Pa]
basilar membrane (BM)	2×10^7
tectorial membrane (TM)	3×10^3
Hensen cells	3×10^3
inner hair cell (IHC)	3×10^3
outer hair cells (OHC)	1×10^5
Deiters cells	3×10^3
Deiters cell rod	1×10^8
spiral ligament	1×10^9
spiral lamina	1×10^9
spiral limbus	1×10^6
pillar cell head	1×10^7
outer/inner pillar cells	1×10^8
reticular lamina (RL)	3×10^8
inner sulcus	3×10^3
stereocilia	1×10^5

need to be carefully tuned when used to model other positions along the cochlea.

3. Motion in the organ of Corti

3.1. Coordinates and sign conventions

The cross section of the cochlea contains the BM, TM, OHCs, RL and other types of cells, reflecting its complex geometry and composition. It is necessary to define local coordinates and a sign convention for describing the motion within the fine structures of the cochlear. In order to compare simulation results with those measured in experiments, we assume that vertical motion is normal to the observing surface, whereas radial motion is perpendicular to the vertical motion, as shown in figure 2 for different observing components. Upward vertical motion is defined to be positive, which corresponds to motion towards the scala vestibuli. These definitions are similar to those used in experiments [9,11], which enables us to directly compare model prediction with them. It is difficult to exactly match the coordinate system in the model with that of the experiments, however, so that there may always be some angle between these two coordinate systems.

3.2. Static response

As a preliminary validation of the overall material properties and geometry of the model, the static elastic response is first calculated, to compare with experimental observation [6] and other numerical models [29]. A positive static pressure loading, in the scala tympani, is uniformly applied at the bottom of the BM corresponding to a negative pressure difference between the scala media and the scala tympani.

Under the influence of this static pressure, the whole organ of Corti moves towards the scala vestibuli, as shown in figure 3. The BM shows a slightly asymmetric radial
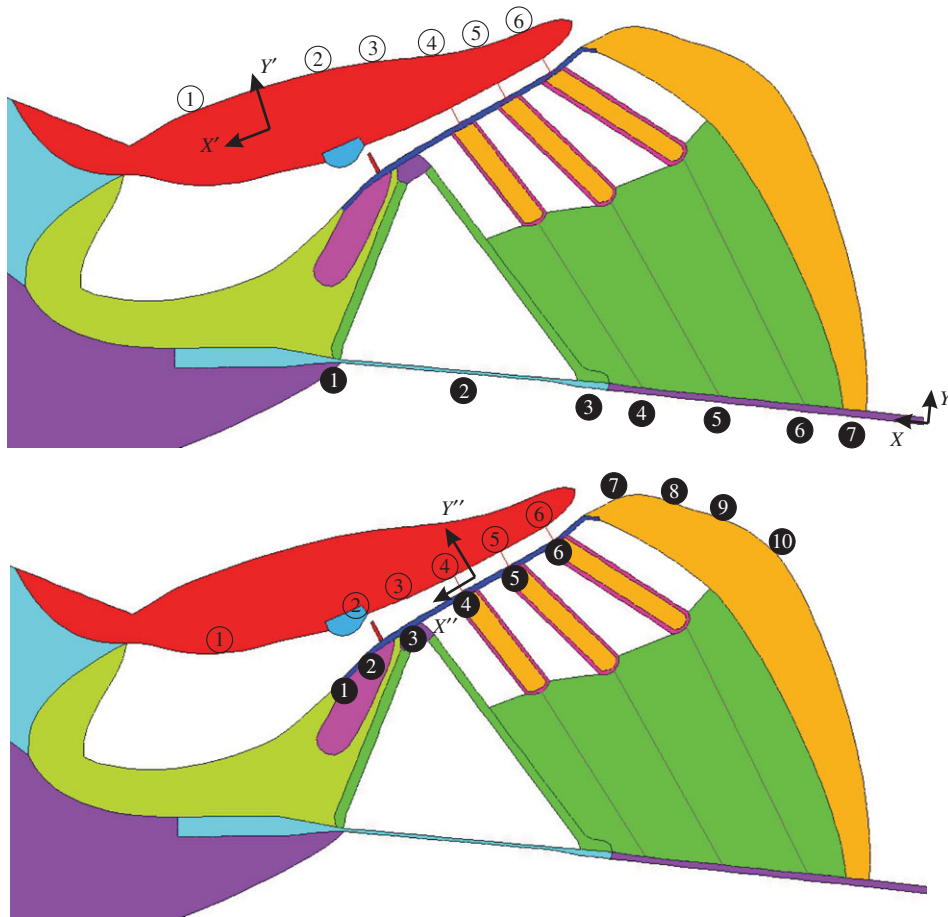
Figure 2. Observation points and local coordinates of the cochlear partition for acoustic and electrical stimulus. Y, Y' and Y'' show directions perpendicular to the BM, TM and RL, and X, X' and X'' show directions along the BM, TM and RL. These local coordinates are defined according to those used in experiments [9,11].
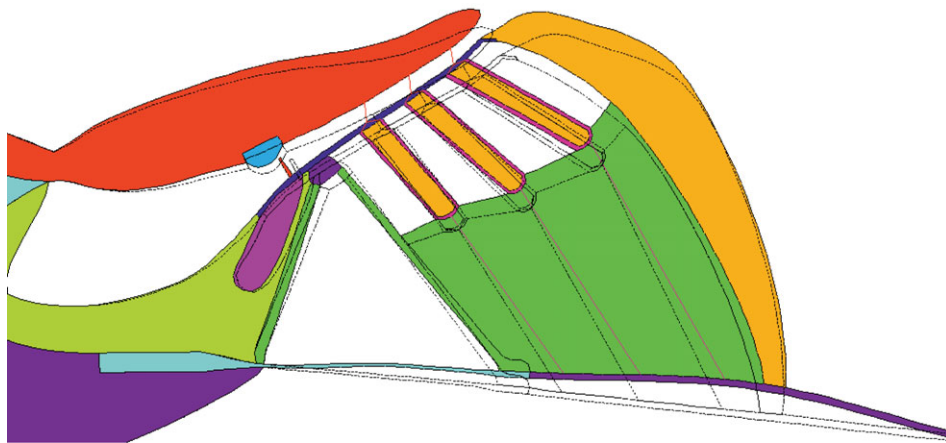

Figure 3. An exaggerated organ of Corti deflection plot due to a positive static pressure loading on the BM in the scala tympani and the undeformed shape is shown light (animation in electronic supplementary material).

mode shape, with maximum displacement around the third row of the OHCs. The RL moves as a stiff plate without much bending and is pivoting around a point close to the inner hair cell (IHC). The magnitude of the RL displacement grows linearly from the IHC towards the third row of the OHCs. A relative shearing motion can also be observed between the TM and the RL, as seen in the deflection of the OHCs stereocilia. The displacement pattern of the results from this two-dimensional slice model qualitatively agree with those from the experiment reported by Fridberger *et al.* [6] and the numerical model reported by Steele *et al.* [29].

3.3. Dynamic response to acoustic stimulus

To simulate sound-induced motion within the organ of Corti, a sinusoidal pressure difference is applied uniformly across the BM at different frequencies. Figure 4 shows the resulting motion at different positions within the organ of Corti as a function of excitation frequency. This indicates that the RL moves as a rigid plate pivoting against a point close to the IHC at low frequencies, because the different parts of the RL all move in phase. The displacement close to the IHC shows the smallest amplitude. The TM upper surface moves as a unit at low frequencies as well, below about 1 kHz, each
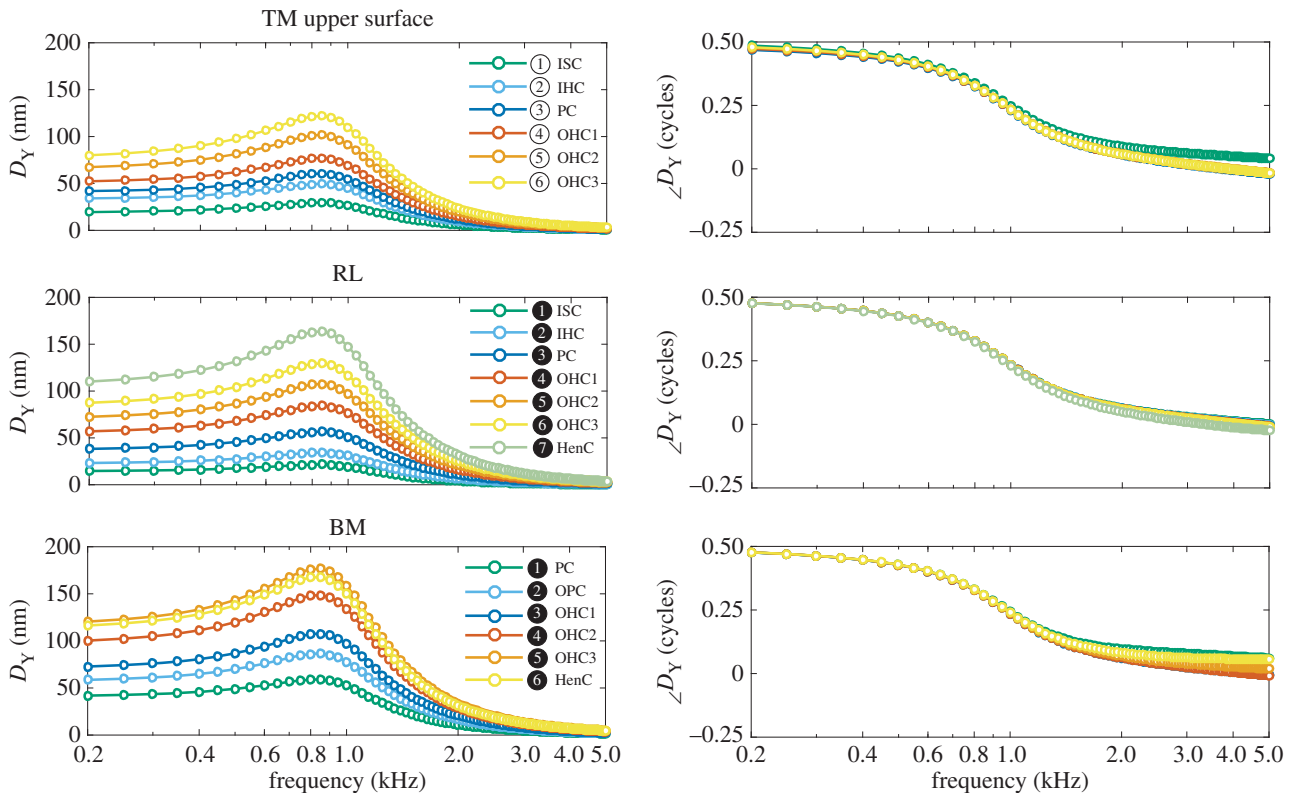
Figure 4. Vertical displacement, normal to surface and phase, relative to the driving pressure difference, of the TM upper surface, the RL and the BM at different positions along their radial length at different frequencies when driven by an acoustic stimulus of 1 Pa. (ISC, inner sulcus; IHC, inner hair cell; PC, pillar cell; OPC, outer pillar cell; OHC, outer hair cell; HenC, Hensen cells, as numbered in figure 2.) (Online version in colour.)
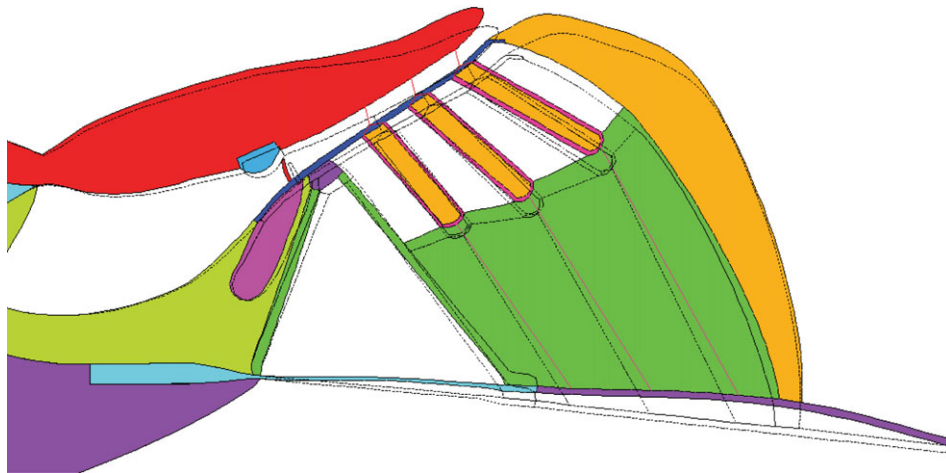

Figure 5. An exaggerated deflection plot inside the organ of Corti when the BM is driven by a pressure difference loading at 0.8 kHz (animation in electronic supplementary material).

position moving in phase. BM motion shows a first-order bending mode, which is similar to that with the static pressure loading. The displacement peak at resonance in this single slice is, however, considerably less than the overall maximum displacement that occurs in the fully coupled cochlea, because the latter is due to the enhancement of the travelling wave over some longitudinal distance, as discussed above. To compare with experimental measurements [7,11], we focus on motion at the characteristic frequency. It should be noted that at this stage the model is only capable of reproducing the passive response to acoustic stimulus and care needs to be taken when comparing the results with those obtained from *in vitro* measurements [7,11], in which the cochlea

remains partially active, and the degree of activity may not be well controlled [3].

Figure 5 shows a plot of displacement in response to a sinusoidal acoustic stimulus at 0.8 kHz, which is approximately the same as the characteristic frequency of the cochlear slice. The TM moves as a single unit and the overall displacement gradually increases outward to the point at the outermost extent and is minimal at the spiral lamina end. The BM displacements increase linearly from the feet of the IHC to the feet of the outer pillar cells and the amplitude peaks close to the third row of the OHCs. The pivot point of the BM is at the feet of the inner pillar cells. The TM displacement is about 0.6 of the BM, which is close to non-invasive
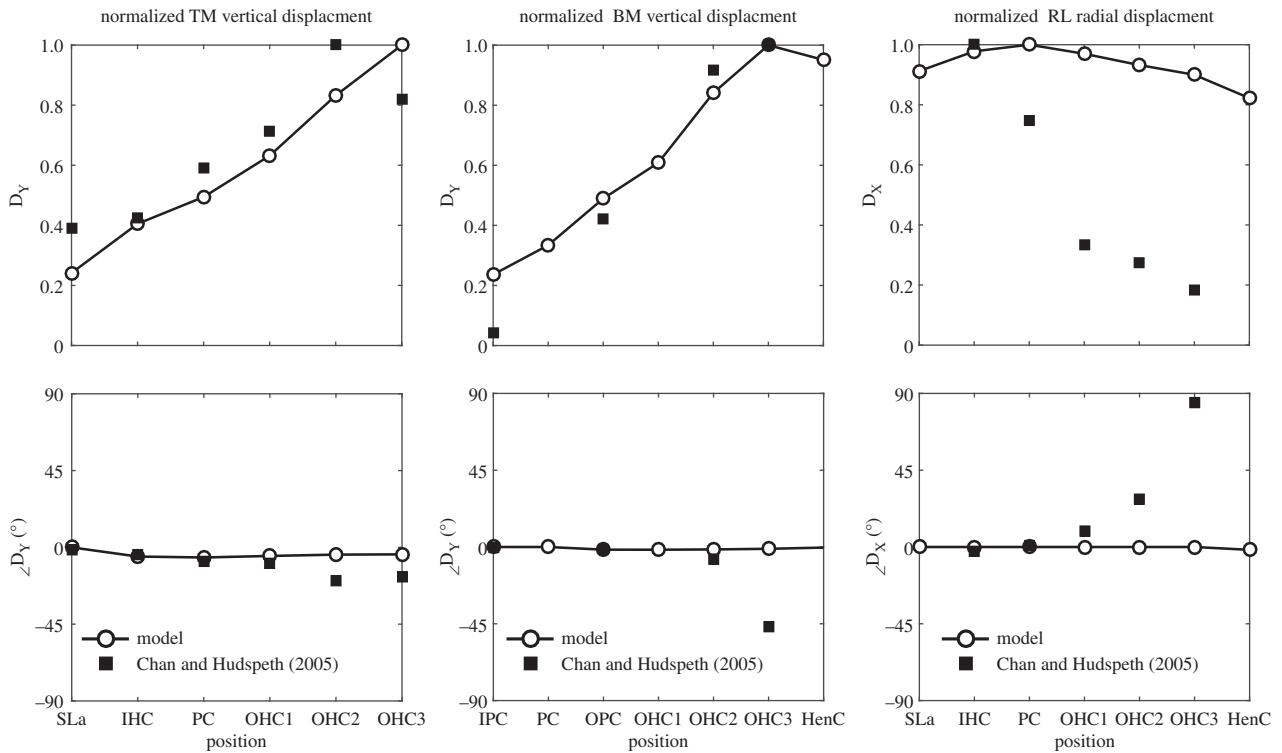
Figure 6. Responses of the organ of Corti to an acoustic stimulus at 0.8 kHz, together with those taken from figs. 1 and 2 in Chan & Hudspeth [11] (square) normalized with respect to the maximum value. TM vertical displacement and phases relative to that at the spiral lamina (left), normalized BM vertical displacement and phases relative to that at the inner pillar cells (middle) and normalized RL radial displacement and phase relative to that at the spiral lamina (right). (Sla, spiral lamina; IHC, inner hair cell; IPC, inner pillar cell; PC, pillar cell head; OPC, outer pillar cell; OHC, outer hair cell; HenC, Hensen cells.)

measurement of a nearly passive cochlea at high sound intensities [9].

The RL also shows a pivoting motion with the centre close to the IHC region. Displacements of the RL increase linearly in the direction of the OHCs. The OHC displacements have similar orientation, which implies that OHCs are barely deformed. These are consistent with the observations of Fridberger & Boutet de Monvel [7], in which motion within the organ of Corti was measured under passive condition. This was ensured by a high-level excitation and a drug to block the OHC electromotility. A clear shear motion of the stereocilia can also be seen in figure 5, in which inward radial motion of structures along the RL leads to outward deflection of hair bundles.

Detailed motion patterns at different position along the RL, TM and BM are plotted in figure 6, to compare with those observed by Chan & Hudspeth [11]. The vertical motion, in the y-direction, is perpendicular to the surface of RL, TM or BM, which are positive for movement towards the scala vestibuli.

Although the measuring positions might be at slightly different positions in the model and in the experiment, they still show a reasonable qualitative agreement. The predicted TM vertical displacement shows good agreement with those from the experiment, in both amplitude and phase. The BM vertical displacement was measured with fewer positions in the experiment and begins to show a phase difference compared with the model at positions beyond the second row of OHCs. The predicted amplitude of the radial response of the RL shows a significant difference with that measured in these experiments. The decrease from the innermost position to the outmost position that was observed in the experiment is not present in the model,

which may be caused by some remaining OHC motility in the experiment.

3.4. Dynamic response to electrical stimulus

In order to study the effect of OHC somatic electromotility, a sinusoidal voltage is applied, in phase, across the walls of each OHC, which are modelled using piezoelectric elements. The thickness of the OHC wall will thus be modulated, which changes the axial length of the cell, because the intracellular fluid is nearly incompressible. The OHCs elongation and contraction correspond to polarization and depolarization, and these simulation results are compared with experiments in which the OHCs are driven electrically.

There are several significant phenomena that are observed when the model is driven electrically. First, the resonant frequency in the case of electrical excitation is about 1.2 kHz, which is about a half octave higher than that in the passive acoustic case, as will be illustrated in figure 10. The increase in resonant frequency may be because the fluid loading on the organ of Corti, when driven electrically is less than when driven acoustically, because less fluid is displaced [52]. In the case of electrical excitation, parts of the BM move up, while another part moves down and consequently less fluid has to be moved further away from the BM in comparison with the in phase motion of the BM for the pressure load. Second, the RL motion at the IHC is out of phase with that at the second row of the OHCs (OHC2), as shown in figure 7. This is consistent with the measurements of Nowotny & Gummer ([9], figure 6a,b for example) for the mechanical responses of the organ of Corti of the guinea pig cochlea, at the characteristic frequency, to electrical
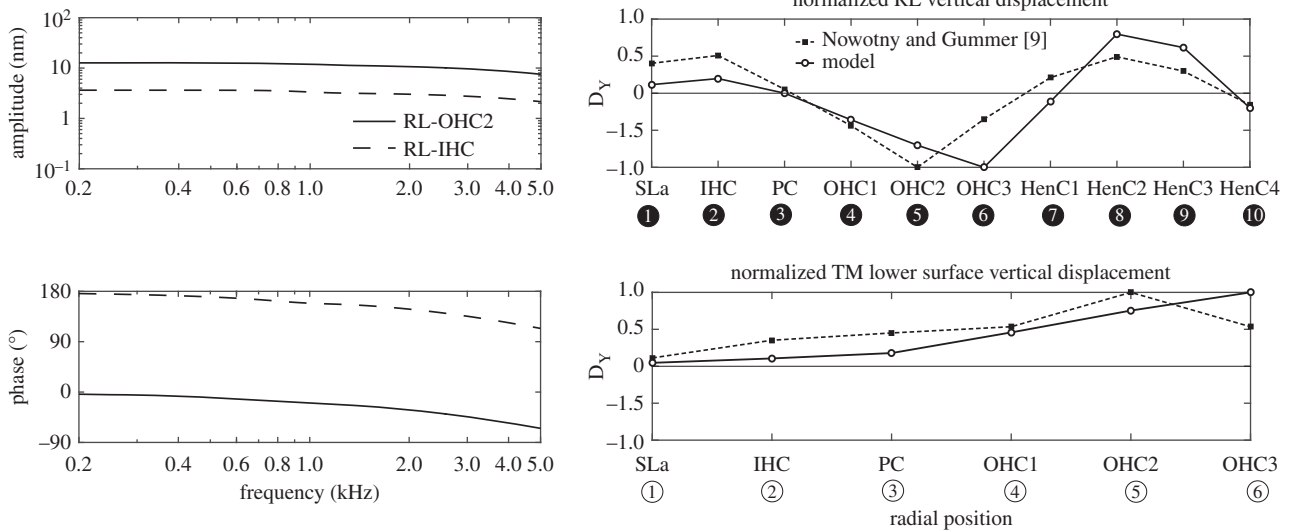
Figure 7. Amplitudes and phases (left column) of the RL vertical displacement at the IHC (RL − IHC) and at the second row of OHCs (RL − OHC2), when the model is driven electrically at different frequencies. The motion patterns at 1.2 kHz of the RL and the lower surface of the TM (right column) together with those measured by Nowotny & Gummer [9] at characteristic frequency, 0.8 kHz. (Sla, spiral lamina; IHC, Inner hair cell; PC, pillar cell head; OPC, outer pillar cell; OHC, outer hair cell; HenC, Hensen cells, numbered as in figure 2.)
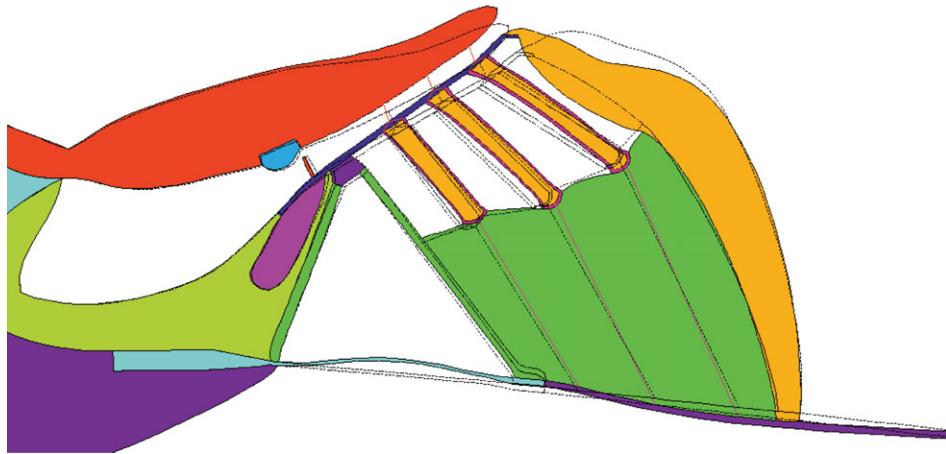
Figure 8. The exaggerated deflection plot inside the organ of Corti when the OHCs are elongated due to electrical excitation at 1.2 kHz (animation in electronic supplementary material).

excitation *in vitro*. Third, the RL and the BM are moving in opposite directions when the OHCs expand, as shown in figure 8. The largest motions are found in the OHC region, where the OHC electromechanical force is coupled directly to the RL and, thus drives the other regions of the organ of Corti, in agreement with the experimental observation [9].

The RL motion at the IHC is predicted to be about 11 dB smaller than at the second row of the OHCs (OHC2), as shown in figure 7, which is in a similar range to that measured by Nowotny & Gummer [9], in which the difference is 7.8 ± 5.7 dB in the third turn of the guinea pig cochlea. The predicted vibration patterns of the RL and the TM in response to electrical stimulation are also shown in figure 7, together with the vibration patterns taken from fig. 2A in [9]. The TM is seen to show in-phase vertical motion along its long axis in agreement with the experimental data. The simulation results of the RL vertical displacements over all observed radial positions show similar vibration patterns to the experiment, except that the RL peak occurs at the second row of OHCs in the experiment rather than at the third row of OHCs in the simulation.

Figure 8 shows a plot of the overall deformation within the organ of Corti in response to OHCs electrical excitation at 1.2 kHz, which is similar to that seen for excitation at 0.8 kHz. Unlike for the passive acoustic excitation, the normal TM displacement is greater than the BM displacement [11]. Furthermore, the BM exhibits a second-order bending mode, which is in contrast to the first-order mode in the passive case. The arcuate and pectinate zones of the BM move out of phase with each other, as observed by Nuttall *et al.* [53] in the *in vivo* measurement of electrically driven BM movements in the guinea pig cochlea.

4. Fully active linear response to acoustic stimulus

The active process within the organ of Corti, created by the somatic motility of the OHCs, can be represented using a block diagram, as shown in figure 9.

With no OHC feedback and assuming linearity, the BM displacement, w_{BM}, and the average shear motion of the
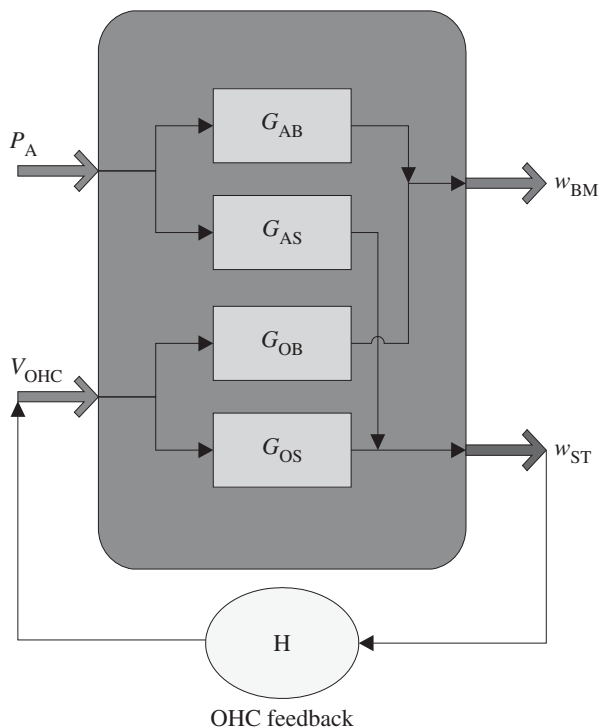
Figure 9. Block diagram of the cochlear electromechanical feedback system. The organ of Corti vibration due to either acoustic or electrical stimulation produce both BM motion, w_{BM}, and a shear motion, w_{ST}, between the RL and the TM at the middle OHCs position in proportion to the receptances G_{AB}, G_{AS}, G_{OB} and G_{OS}. The shear motion of the OHC stereocilia, w_{ST}, is assumed to generate the active OHCs force via the OHC frequency response, H.

OHC stereocilia, w_{ST}, can be written as the superposition of responses due to the acoustic pressure difference excitation, P_A, and the electrical excitation due to all the OHCs, V_{OHC},

$$w_{BM} = G_{AB}P_A + G_{OB}V_{OHC} \qquad (4.1)$$

and

$$w_{ST} = G_{AS}P_A + G_{OS}V_{OHC}, \qquad (4.2)$$

where a negative pressure difference P_A or positive V_{OHC}, driving a contraction of the OHC, generates an upward w_{BM}. In the simulation all three OHCs are driven with the same voltage, V_{OHC}. The complex transfer responses G_{AB}, G_{AS}, G_{OB} and G_{OS} represent the receptances (displacement per unit pressure or voltage) of the BM motion, and of the shearing motion between the TM and RL, when driven either acoustically, by pressure difference P_A, or electrically, by V_{OHC}.

The action of the OHCs is shown as a feedback path in figure 9: from the stereocilia shear displacement, w_{ST}, to the OHC electrically excitation, V_{OHC}. In normal forward transduction, the stereocilia of the OHCs convert mechanical stimuli into electrical responses. In reverse transduction, the voltage inside the OHCs evokes a mechanical response. These two forms of transduction are combined together into an overall OHC feedback path in figure 9. The frequency responses of the individual receptances (in figure 9) can be calculated from the passive finite-element model and these are plotted in figure 10. The response of the BM due to acoustic excitation, G_{AB}, clearly shows the characteristic frequency of this slice model, which is around 0.8 kHz, although other well-damped resonances also contribute to all the responses. Its response to electrical excitation, G_{OB}, shows a resonance at

Table 2. Value for the electrical parameters used in the OHC feedback loop in the slice model [30].

parameter	value	unit
γ	0.9: active	—
	0: passive	
g	7.2×10^7	V m^{-1}
$1/R_m$	1.3	mS m^{-1}
C_m	3.7	μF m^{-1}

about 1.2 kHz, however, which is about half an octave above the characteristic frequency, as noted above.

In the closed loop, the OHC tresponse due to the feedback is defined to be

$$V_{OHC} = Hw_{ST}, \qquad (4.3)$$

where H is a complex feedback response, which depends on the properties of the OHCs. A simple model of this feedback response [30,54] is given by

$$H = \frac{\gamma g}{1 + i\omega R_m C_m}, \qquad (4.4)$$

where γ is the normalized level of active amplification, R_m is the OHC electrical resistance, C_m is its electrical capacitance and g is an overall gain. This overall gain is chosen so that the closed loop system is on the edge of instability with $\gamma = 1$, as calculated by plotting the Nyquist plot of $G_{OS}(i\omega)H(i\omega)$, in which $G_{OS}(i\omega)$ has been calculated up to 20 kHz to complete this plot. The stability properties of this isolated slice will be different to those of the coupled cochlea, but because even the most sensitive slice preparation has not been observed to spontaneously oscillate, it is reasonable to assume that an appropriate value of feedback gain is below that which causes instability, and a value of $\gamma = 0.9$ has been used here to represent the fully active cochlea. The values of the assumed OHC parameters are listed in table 2.

Substituting equation (4.3) into (4.2) allows the closed loop OHC response to be calculated, when driven by the acoustic excitation, as

$$V_{OHC} = \frac{G_{AS}H}{1 - G_{OS}H}P_A. \qquad (4.5)$$

The BM displacement, w_{BM}, in the closed loop is thus given, using equation (4.1), as

$$w_{BM} = \left(G_{AB} + G_{OB}\frac{G_{AS}H}{1 - G_{OS}H}\right)P_A. \qquad (4.6)$$

Equation (4.5) can be used to predict the fully active response of the BM, using the individual responses calculated from the passive finite-element model and the assumed OHC response.

It should be noted that at low frequencies H is positive, because an excitatory displacement of the OHC stereocilia generates a positive current and hence a positive voltage, depolarization, in the OHC. G_{OS} is negative, however, because a positive OHC voltage causes it to contract and so move the stereocilia in the inhibitory direction. The feedback loop formed by the OHCs thus generates negative feedback at low frequencies, as emphasized by Khanna & Hao [55] and Lu *et al*. [56] for example.
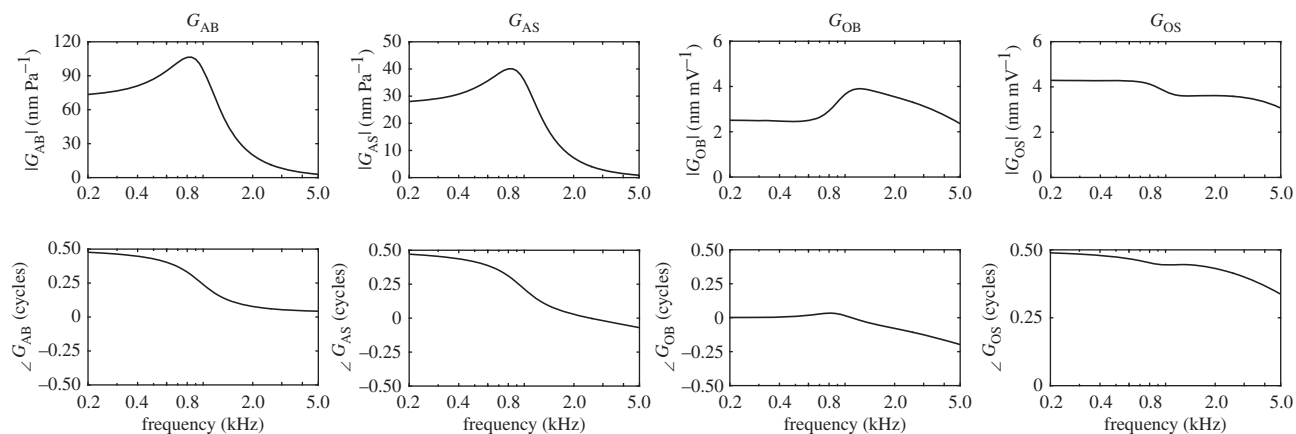
Figure 10. The receptances of the BM motion and of the shear motion of the OHC stereocilia, obtained when the finite-element model is driven either acoustically, G_{AB} and G_{AS}, or electrically, G_{OB} and G_{OS}.
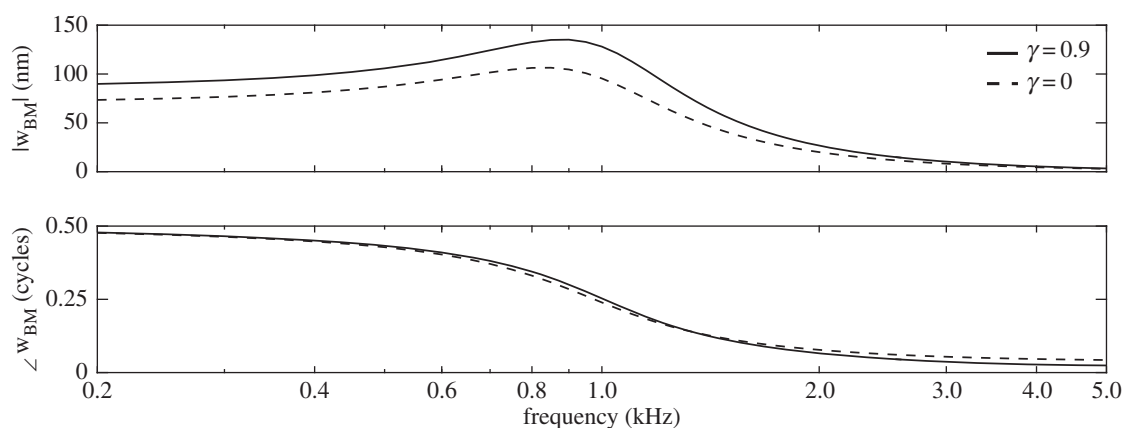
Figure 11. The passive frequency response of the BM displacement in the two-dimensional slice model due to the acoustic pressure, $G_{AB}P_A$, and the calculated active response in the closed loop with $\gamma = 0.9$, calculated with 1 Pa acoustic pressure excitation.
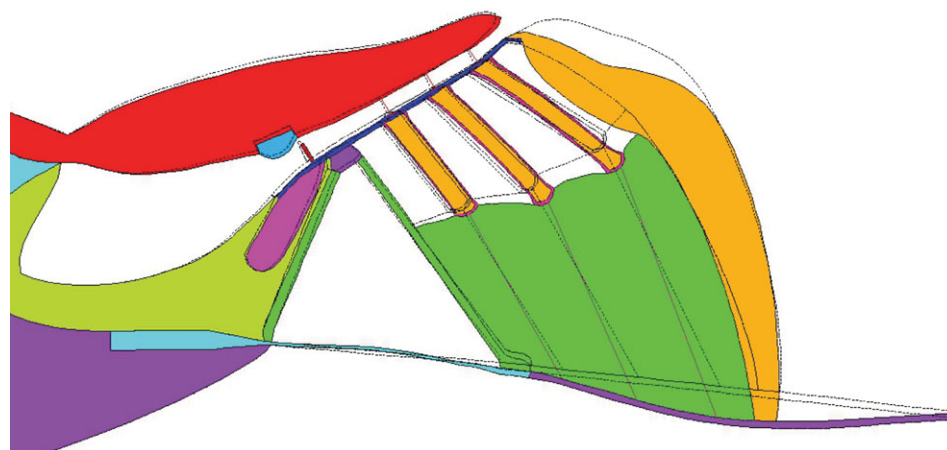
Figure 12. The exaggerated deflection plot inside the organ of Corti, calculated with 1 Pa acoustic pressure excitation at 0.85 kHz, when the OC is under fully active condition (animation in electronic supplementary material).

Figure 11 shows the magnitude and phase of the BM displacements, calculated using equation (4.6), in response to acoustic excitation when the system is passive, $\gamma = 0$, and active, $\gamma = 0.9$. In the active case, the amplitude of the RL in the OHC region falls by about 54%, whereas the peak BM response is predicted to be about 27% greater than that of the passive model. In the measurements of Fridberger & Boutet de Monvel [7], when a drug is not used to block OHC electromotility, the amplitudes of the RL fall by about 32%, whereas the amplitudes of the BM increase by 50%

comparing with a passive cochlea. It should be emphasized, however, that the amplification in a single slice will not be the same as that seen in the coupled cochlea, where the activity of the cochlea basal to the characteristic place has been shown to significantly amplify the passing wave [57,58]. The internal motion of the organ of Corti under the fully active condition is calculated by adding together that due to a purely acoustic excitation and that due to an OHC voltage excitation given by equation (4.5), as shown in figure 12, and a movie of this is included in the electronic supplementary material, as are

movies for the static pressure loading, the individual acoustic and electrical stimulations. The relative internal motion under the fully active condition is seen to be quite similar to that for just electrical stimulation, indicating that the OHC somatic forces make a significantly larger contribution to the BM movement than the acoustic pressure alone, even though the former is required to initiate motion. The radial distribution of BM displacement is similar to that observed in [59]. It is striking that the deflection of the OHC's stereocilia is significantly reduced, by about 20 dB, by the action of the feedback loop, as seen in the animation of the fully active cochlea in figure 12. This can only be achieved if the normal motion of the RL is also smaller in this position. The OHCs are driven quite hard to maintain this condition, however, so that the RL motion above the IHCs still has significant motion. Unfortunately, this two-dimensional simulation does not give a realistic prediction of the motion of the IHC stereocilia, due to the flow of fluid in the subtectorial space, so no conclusions can be drawn at this stage about the change in IHC excitation under these fully active conditions.

The active response of this two-dimensional model does not completely reflect the biological amplification process in the three-dimensional cochlea, because the slice model does not, for example, include fluid longitudinal coupling, the full three-dimensional orientation of the OHC or the nonlinearity of the OHC response, which are all important to the overall cochlear response. In general, however, this linear combination of the cochlear responses to acoustic and electrical excitations does provide a way of predicting the fully active response of a cochlear slice, as would be observed in *in vitro* experiments at low levels, and can be used to simulate the complete internal motion of the organ of Corti under these conditions.

5. Conclusion

The motions within the organ of Corti have been simulated using a two-dimensional linear finite-element model of a slice of the cochlea, under either acoustic or electrical excitation, and these have been shown to be similar to those observed in experiments. The advantages of the finite-element models are

its power of incorporating detailed anatomical structures and the consequent avoidance of the assumptions and simplifications inherent in lumped-parameter models [31,32,54].

A linear combination of the responses of our cochlear model to different types of excitation is then used to predict the active linear response to acoustic excitation. The relative motion within the organ of Corti is thus predicted for the fully active cochlear slice model. This formulation allows the active response of the cochlea to be calculated at a relatively low computational cost. It also provides the opportunity of extending this work to take into account the nonlinearity of the OHC. If the nonlinearity is assumed to be confined to the OHC electromotility, so that the individual receptances within figure 9 remain linear, time domain versions of these responses can be calculated based on the computed frequency responses. This opens up the possibility of nonlinear time domain simulations of the organ of Corti, using a nonlinear model of the OHC response. The effect of local longitudinal coupling could also be considered by extruding the slice into a three-dimensional segment, with a finite length in the longitudinal direction. Ultimately, wave propagation could be modelled, either using a full three-dimensional model of the entire cochlea, or by coupling the local responses of a number of micromechanical segments with an overall fluid coupling model. The behaviour of the local feedback within each slice, when coupled to the responses of adjoining slices could then be predicted, to help understand the transmission of wave energy along the cochlea. In this way, modelling methods could be used to complement the existing experimental measurements and further contribute to our understanding of the mechanics of the cochlea.

References

1. von Békésy G. 1970 Travelling waves as frequency analysers in the cochlea. *Nature* **225**, 1207–1209. (doi:10.1038/2251207a0)

2. de Boer E, Viergever MA. 1984 Wave propagation and dispersion in the cochlea. *Hear. Res.* **13**, 101–112. (doi:10.1016/0378-5955(84)90101-1)

3. Robles L, Ruggero MA. 2001 Mechanics of the mammalian cochlea. *Physiol. Rev.* **81**, 1305–1352.

4. Lee HY, Raphael PD, Park J, Ellerbee AK, Applegate BE, Oghalai JS. 2015 Noninvasive *in vivo* imaging reveals differences between tectorial membrane and basilar membrane traveling waves in the mouse cochlea. *Proc. Natl Acad. Sci. USA* **112**, 3128–3133. (doi:10.1073/pnas.1500038112)

5. Nilsen KE, Russell IJ. 2000 The spatial and temporal representation of a tone on the guinea pig basilar membrane. *Proc. Natl Acad. Sci. USA* **97**, 11751–11758. (doi:10.1073/pnas.97.22.11751)

6. Fridberger A, Boutet de Monvel J, Ulfendahl M. 2002 Internal shearing within the hearing organ evoked by basilar membrane motion. *J. Neurosci.* **22**, 9850–9857.

7. Fridberger A, Boutet de Monvel J. 2003 Sound-induced differential motion within the hearing organ. *Nat. Neurosci.* **6**, 446–448. (doi:10.1038/nn1047)

8. Fridberger A, Boutet de Monvel J, Zheng J, Hu N, Zou Y, Ren T, Nuttall A. 2004 Organ of Corti potentials and the motion of the basilar membrane. *J. Neurosci.* **24**, 10057–10063. (doi:10.1523/jneurosci.2711-04.2004)

9. Nowotny M, Gummer AW. 2011 Vibration responses of the organ of Corti and the tectorial membrane to

electrical stimulation. *J. Acoust. Soc. Am.* **130**, 3852–3872. (doi:10.1121/1.3651822)

10. Nowotny M, Gummer AW. 2006 Nanomechanics of the subtectorial space caused by electromechanics of cochlear outer hair cells. *Proc. Natl Acad. Sci. USA* **103**, 2120–2125. (doi:10.1073/pnas.0511125103)

11. Chan DK, Hudspeth AJ. 2005 Mechanical responses of the organ of Corti to acoustic and electrical stimulation *in vitro*. *Biophys. J.* **89**, 4382–4395. (doi:10.1529/biophysj.105.070474)

12. Crawford AC, Fettiplace R. 1985 The mechanical properties of ciliary bundles of turtle cochlear hair cells. *J. Physiol.* **364**, 359–379. (doi:10.1113/jphysiol.1985.sp015750)

13. Martin P, Bozovic D, Choe Y, Hudspeth AJ. 2003 Spontaneous oscillation by hair bundles

of the bullfrog's sacculus. *J. Neurosci.* **23**, 4533–4548.

14. Kennedy HJ, Crawford AC, Fettiplace R. 2005 Force generation by mammalian hair bundles supports a role in cochlear amplification. *Nature* **433**, 880–883. (doi:10.1038/nature03367)

15. Sul B, Iwasa KH. 2009 Effectiveness of hair bundle motility as the cochlear amplifier. *Biophys. J.* **97**, 2653–2663. (doi:10.1016/j.bpj.2009.08.039)

16. Meaud J, Grosh K. 2011 Coupling active hair bundle mechanics, fast adaptation, and somatic motility in a cochlear model. *Biophys. J.* **100**, 2576–2585. (doi:10.1016/j.bpj.2011.04.049)

17. Nin F, Reichenbach T, Fisher JAN, Hudspeth AJ. 2012 Contribution of active hair-bundle motility to nonlinear amplification in the mammalian cochlea. *Proc. Natl Acad. Sci. USA* **109**, 21 076–21 080. (doi:10.1073/pnas.1219379110)

18. Reichenbach T, Hudspeth AJ. 2014 The physics of hearing: fluid mechanics and the active process of the inner ear. *Rep. Prog. Phys.* **77**, 076601. (doi:10.1088/0034-4885/77/7/076601)

19. Mellado Lagarde MM, Drexl M, Lukashkina VA, Lukashkin AN, Russell IJ. 2008 Outer hair cell somatic, not hair bundle, motility is the basis of the cochlear amplifier. *Nat. Neurosci.* **11**, 746–748. (doi:10.1038/nn.2129)

20. Kolston PJ. 1999 Comparing *in vitro*, *in situ*, and *in vivo* experimental data in a three-dimensional model of mammalian cochlear mechanics. *Proc. Natl Acad. Sci. USA* **96**, 3676–3681. (doi:10.1073/pnas.96.7.3676)

21. Kolston PJ, Ashmore JF. 1996 Finite element micromechanical modeling of the cochlea in three dimensions. *J. Acoust. Soc. Am.* **99**, 455–467. (doi:10.1121/1.414557)

22. Nam J-H, Fettiplace R. 2010 Force transmission in the organ of Corti micromachine. *Biophys. J.* **98**, 2813–2821. (doi:10.1016/j.bpj.2010.03.052)

23. Nam J-H. 2014 Microstructures in the organ of Corti help outer hair cells form traveling waves along the cochlear coil. *Biophys. J.* **106**, 2426–2433. (doi:10.1016/j.bpj.2014.04.018)

24. Andoh M, Wada H. 2004 Prediction of the characteristics of two types of pressure waves in the cochlea: theoretical considerations. *J. Acoust. Soc. Am.* **116**, 417–425. (doi:10.1121/1.1763599)

25. Andoh M, Nakajima C, Wada H. 2005 Phase of neural excitation relative to basilar membrane motion in the organ of Corti: theoretical considerations. *J. Acoust. Soc. Am.* **118**, 1554–1565. (doi:10.1121/1.2000770)

26. Chihiro N, Masayoshi A, Hiroshi W. 2005 Finite-element analysis of the auditory transduction process in the guinea pig cochlea. In *Twelfth Int. Congr. on Sound and Vibration, Lisbon, Portugal, 11–14 July*, p. 7.

27. Cai H, Chadwick R. 2003 Radial structure of traveling waves in the inner ear. *SIAM J. Appl. Math.* **63**, 1105–1120. (doi:10.1137/S0036139901388957)

28. Cai H, Shoelson B, Chadwick RS. 2004 Evidence of tectorial membrane radial motion in a propagating mode of a complex cochlear model. *Proc. Natl Acad.*

Sci. USA. **101**, 6243–6248. (doi:10.1073/pnas.0401395101)

29. Steele CR, de Monvel JB, Puria S. 2009 A multiscale model of the organ of Corti. *J. Mech. Mater. Struct.* **4**, 755–778. (doi:10.2140/jomms.2009.4.755)

30. Ramamoorthy S, Deo NV, Grosh K. 2007 A mechano-electro-acoustical model for the cochlea: response to acoustic stimuli. *J. Acoust. Soc. Am.* **121**, 2758–2773. (doi:10.1121/1.2713725)

31. Neely ST, Kim DO. 1986 A model for active elements in cochlear biomechanics. *J. Acoust. Soc. Am.* **79**, 1472–1480. (doi:10.1121/1.393674)

32. Elliott SJ, Pierzycki R, Lineton B. 2006 Lumped-parameter models for cochlear micromechanics. In *ISVR Technical Memorandum 967, University of Southampton, November*, p. 33.

33. Böhnke F, Arnold W. 1998 Nonlinear mechanics of the organ of Corti caused by Deiters cells. *IEEE Trans. Biomed. Eng.* **45**, 1227–1233. (doi:10.1109/10.720200)

34. Lim K, Steele CR. 2002 A three-dimensional nonlinear active cochlear model analyzed by the WKB-numeric method. *Hear. Res.* **170**, 190–205. (doi:10.1016/S0378-5955(02)00491-4)

35. Yoon YJ, Steele CR, Puria S. 2011 Feed-forward and feed-backward amplification model from cochlear cytoarchitecture: an interspecies comparison. *Biophys. J.* **100**, 1–10. (doi:10.1016/j.bpj.2010.11.039)

36. Wang X, Wang L, Zhou J, Hu Y. 2014 Finite element modelling of human auditory periphery including a feed-forward amplification of the cochlea. *Comput. Methods Biomech. Biomed. Eng.* **17**, 1096–1107. (doi:10.1080/10255842.2012.737458)

37. Baumgart J, Chiaradia C, Fleischer M, Yarin Y, Grundmann R, Gummer AW. 2008 Fluid mechanics in the subtectorial space. In *Concepts and challenges in the biophysics of hearing, Proc. 10th Int. Workshop on the Mechanics of Hearing* (eds NP Cooper, DT Kemp), pp. 288–293. Staffordshire, UK: Keele University, World Scientific.

38. Kozlov AS, Baumgart J, Risler T, Versteegh CPC, Hudspeth AJ. 2011 Forces between clustered stereocilia minimize friction in the ear on a subnanometre scale. *Nature* **474**, 376–379. (doi:10.1038/nature10073)

39. Baumgart J. 2010 *The hair bundle: fluid–structure interaction in the inner ear.* PhD thesis, Technische Universität Dresden, Dresden.

40. de Boer E. 1996 Mechanics of the cochlea: modelling efforts. In *The cochlea* (eds P Dallos, AN Popper, RR Fay), pp. 258–317. New York, NY: Springer.

41. Elliott SJ, Lineton B, Ni G. 2011 Fluid coupling in a discrete model of cochlear mechanics. *J. Acoust. Soc. Am.* **130**, 1441–1451. (doi:10.1121/1.3607420)

42. LeMasurier M, Gillespie PG. 2005 Hair-cell mechanotransduction and cochlear amplification. *Neuron* **48**, 403–415. (doi:10.1016/j.neuron.2005.10.017)

43. Zienkiewicz OC, Taylor RL. 1994 *The finite element method. Volume 1, Basic formulation and linear problems.* London, UK: McGraw-Hill.

44. Homer M, Champneys A, Hunt G, Cooper N. 2004 Mathematical modeling of the radial profile of basilar

membrane vibrations in the inner ear. *J. Acoust. Soc. Am.* **116**, 1025–1034. (doi:10.1121/1.1771571)

45. Cooper NP. 1999 Radial variation in the vibrations of the cochlear partition. In *Recent developments in auditory mechanics* (eds H Wada, T Takasaka, K Ikeda, T Koike), pp. 109–115. Singapore: World Scientific.

46. Steele CR, Puria S. 2005 Force on inner hair cell cilia. *Int. J. Solids Struct.* **42**, 5887–5904. (doi:10.1016/j.ijsolstr.2005.03.056)

47. Ni G, Elliott SJ. 2013 Effect of basilar membrane radial velocity profile on fluid coupling in the cochlea. *J. Acoust. Soc. Am.* **133**, EL181–EL187. (doi:10.1121/1.4789863)

48. Steele CR, Baker GJ, Tolomeo JA, Zetes-Tolometo DE. 2000 Cochlear mechanics. In *The biomedical engineering handbook* (ed. JD Bronzino), p. 3024. Boca Raton, FL: CRC Press.

49. Scherer MP, Gummer AW. 2004 Vibration pattern of the organ of Corti up to 50 kHz: evidence for resonant electromechanical force. *Proc. Natl Acad. Sci. USA.* **101**, 17 652–17 657. (doi:10.1073/pnas.0408232101)

50. Strelioff D, Flock Å. 1984 Stiffness of sensory-cell hair bundles in the isolated guinea pig cochlea. *Hear. Res.* **15**, 19–28. (doi:10.1016/0378-5955(84) 90221-1)

51. Frank G, Hemmert W, Gummer AW. 1999 Limiting dynamics of high-frequency electromechanical transduction of outer hair cells. *Proc. Natl Acad. Sci. USA* **96**, 4420–4425. (doi:10.1073/pnas.96.8.4420)

52. Elliott SJ, Ni G. 2015 Near field fluid coupling between internal motion of the organ of Corti and the basilar membrane. In *Mechanics of Hearing: Protein to Perception* (eds KD Karavitaki, DP Corey), *23–29 June, Cape Sounio, Greece*, pp. 5. Melville, NY: American Institute of Physics. (doi:10.1063/1.4939353).

53. Nuttall AL, Guo M, Ren T. 1999 The radial pattern of basilar membrane motion evoked by electric stimulation of the cochlea. *Hear. Res.* **131**, 39–46. (doi:10.1016/S0378-5955(99)00009-X)

54. Simón Gálvez MF, Elliott SJ. 2013 Lumped parameter model of the organ of Corti. In *ISVR Technical Memorandum 1000, University of Southampton, August*, p. 55.

55. Khanna SM, Hao LF. 2000 Amplification in the apical turn of the cochlea with negative feedback. *Hear. Res.* **149**, 55–76. (doi:10.1016/S0378-5955(00)00162-3)

56. Lu TK, Zhak S, Dallos P, Sarpeshkar R. 2006 Fast cochlear amplification with slow outer hair cells. *Hear. Res.* **214**, 45–67. (doi:10.1016/j.heares.2006.01.018)

57. Shera CA. 2007 Laser amplification with a twist: traveling-wave propagation and gain functions from throughout the cochlea. *J. Acoust. Soc. Am.* **122**, 2738–2758. (doi:10.1121/1.2783205)

58. Ren T. 2002 Longitudinal pattern of basilar membrane vibration in the sensitive cochlea. *Proc. Natl Acad. Sci. USA* **99**, 17 101–17 106. (doi:10.1073/pnas.262663699)

59. Nilsen KE, Russell IJ. 1999 Timing of cochlear feedback: spatial and temporal representation of a tone across the basilar membrane. *Nat. Neurosci.* **2**, 642–648. (doi:10.1038/12230)